PARAMETRIC INTERTURBINE DUCT DESIGN AND OPTIMISATION

Jürgen Gräsel*, Manuel Pierré*, Jacques Demolis*
***Turbomeca**
Turbine Design Department
F-64511 Bordes/France

Keywords: *optimisation, interturbine duct, parametric design*

Abstract

The objective of the present research is to develop a fast and robust tool for the parametric design and optimisation of S-shaped ducts. In contrast to the inherently three-dimensional nature of the duct flow, current design practice for inter-turbine ducts still employs standard performance maps derived from annular diffusers. As a consequence these low fidelity methods produce duct shapes, which are far from the optimum in terms of minimum duct length and maximum area ratio. The present work aims at improving the design process by extensive use of CFD and the introduction of shape optimisation methods.

Nomenclature

AR	Area ratio
Cp	Pressure recovery coefficient
CCD	Central-Composite Design
DOE	Design of Experiment
HPT	High Pressure Turbine
h	Height
ITD	Intermediate Turbine Duct
L	Duct Length
LHS	Latin Hypercube Sample
LPT	Low Pressure Turbine
m	Number of CFD runs
N	B-spline Basis-polynomial
p	Number of parameters
P	Pressure
PMXC	Position of Maximum Thickness
r	Radius
RSA	Response surface approximation
S	Arc Length
t	B-spline parameter
T/C	Thickness to chord ratio
u	Circumferential velocity
y+	Non-dimensional wall distance
B	Control-point
x	Curve-point
α	Stagger angle
ζ	Total-pressure loss coefficient
ω	Weighting Factor

Subscripts

0	Total
1	Duct Inlet plane
2	Duct Exit plane
ref	Reference

1 Introduction

Helicopter aero engines are small gas turbines which are highly integrated in the helicopter fuselage. The growing demand on weight savings and efficiency gain has resulted in a quest for compact, aerodynamically optimised engines. New blade design methods have been developed in the past to increase the aerodynamic loading and to minimise the profile loss of the blade. Prominent examples for the successful application of these methods are the controlled diffusion compressor aerofoils [1] and ultra high-lift turbine blades [2], which have made their way into modern aero engine design. Only little effort has been put in the advancement of design methods for intermediate turbine ducts (ITD). These S-shaped ducts as shown in figure 1 provide the flowpath from the high-pressure turbine (HPT) discharge to the larger diameter inlet of the low-pressure turbine (LPT). They may also integrate hollow struts, which enclose service tubes and support the bearing housing.

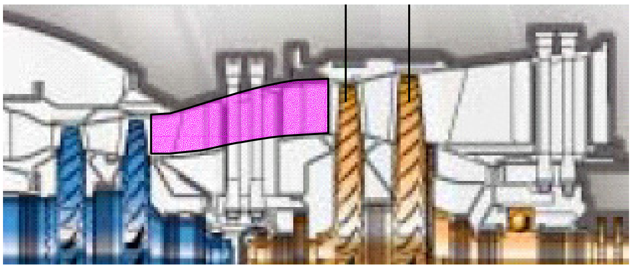

Fig.1. Intermediate duct in a helicopter engine

The radial offset between HPT and LPT increases for a given rotational speed the circumferential speed *u* of the LPT and hence reduces the stage loading coefficient $\Delta H/u^2$. The flow additionally diffuses due to the area increase which decreases the flow coefficient c_{ax}/u. The reduction of both coefficients results in an augmentation of LPT efficiency according to the Smith turbine loading diagram. It has to be noted that in contrast to a turbofan engine with its high-bypass ratio, the HPT-LPT radial offset for a helicopter engine is less pronounced in order to fulfil installation requirements. The length of the ITD is a trade-off between engine weight penalties, the minimum space to accommodate the turbine bearing support and the maximum possible meridional gas path steepness. The latter one is limited by the onset of flow separation in the ITD.

The ITD flowfield is influenced by the upstream high-pressure rotor, the end wall curvature and the strut blockage. The research on interaction mechanisms within the ITD and its neighbouring components has recently received increasing interest with the development of high-bypass turbofan engines [3, 4]. It has been shown by Miller et al [5] that for an unshrouded HPT-rotor the inlet flow is dominated by the rotor-tip leakage flow close to the casing wall and the rotor hub passage vortex. The stator wakes, which are convecting through the rotor rows, generate additionally a pitchwise non-uniform flowfield. The static pressure development through the duct depends on the radius of curvature of the end walls. Due the lower radius of curvature of the casing end wall at the first bend of the S-shaped duct, a radial pressure gradient is generated to counteract the centrifugal force on the fluid. As a result the low momentum hub flow migrates outwards. After the first bend the casing flow decelerates until the second concave bend, which thickens the boundary layer and may cause flow separation.

2 Design of Intermediate Ducts

The preliminary design of intermediate ducts is often based on standard diffuser performance maps, which had been systematically generated from numerous experimental studies. The well known Sovran and Klomp diagram [6] for example determines for a given duct length *L* with an inlet height *h* and an exit to inlet area ratio *AR* the static pressure rise coefficient:

$$C_p = \frac{\overline{P}_2 - \overline{P}_1}{\overline{P}_{01} - \overline{P}_1} \qquad (1)$$

It also serves to classify the ITD as aggressive or non-aggressive with respect to its position above the C_p^* or below the C_p^{**} - line in figure 2.

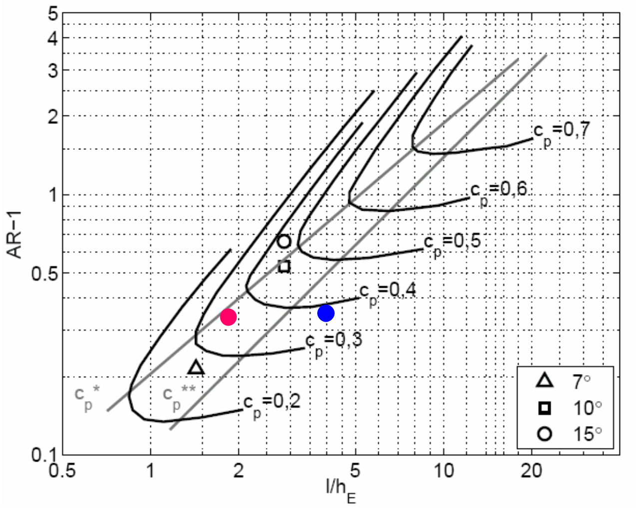

Fig.2. Sovran and Klomp diffuser map from [7]

The maximum pressure recovery is limited by the ideal pressure rise coefficient C_{pi}, which is for non-swirling flow simply a function of *AR:*

$$C_{pi} = 1 - AR^{-2} \qquad (2)$$

However, the effect of flow blockage, strut losses and inlet swirl are not accounted for in eqns. (1) and (2). This means also that the total pressure loss of the duct:

$$\zeta = \frac{\overline{P}_{02} - \overline{P}_{01}}{\overline{P}_{01} - \overline{P}_{1}}, \qquad (3)$$

could not be derived from both C_p values [8]. The next level of design refinement is therefore the inclusion of these parameters in the correlation set for the ITD design.

A systematic computational study for different combinations of these parameters has been carried out in order to create a database for the preliminary duct design. The strut geometry was hereby built from symmetrical aerofoils like the NACA 4-Digit series. All CFD runs have been performed with radial inlet profiles for total pressure, total temperature and swirl. It is assumed that the struts do not alter these profiles [5]. The effect of Mach and Reynolds number on the duct performance has not been considered. Experimental results reported by Feldcamp [9] reveal only a very weak influence of the Reynolds number on C_p and ζ.. Furthermore Vassiliev [10] has shown that the pressure recovery is basically independent of the inlet Mach number. By contrast, the pressure losses increase quadratically with the Mach number.

An example for the result of a CFD run is shown by the total pressure contour distribution in figure 3. The 2D strut shown has a non-zero stagger angle α to match the inlet swirl at the design point.

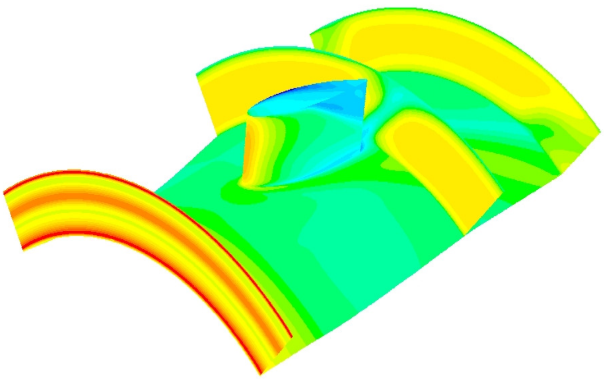

Fig.3. Total Pressure contours of the ITD

The example demonstrates that in the presence of the struts, the resulting flow is inherently three dimensional. The impact of the strut on C_p and ζ depends strongly for a given geometry on the stagger angle α as illustrated in figure 4. This is of specific importance for a turboshaft engine even if the ITD inlet swirl angle change from idle to take-off is far less dramatic than for the exhaust diffuser. As can be observed in figure 4, the wake pattern in the strut exit plane switches form a lambda-structure to a y-structure. The local incidence change from positive at the hub to highly negative at the casing causes flow separation on the leeward side of the strut. The casing boundary layer is slightly thicker in the strut exit plane than the hub boundary layer due to the higher flow deceleration.

The augmentation of the thickness to chord ratio *T/C* results as expected in an increase of the wake thickness and hence ζ.. The wake diffuses circumferentially and merges with the casing end wall. The computations show a linear increase of the pressure loss with *T/C*. The pressure recovery is not affected by the changes in *T/C*. The influence of the position of maximum thickness PMCX on the total pressure loss is yet weak. The number of struts in the duct has also been modified during the study. It was found that the strut number contributes linearly to the global total pressure loss. For the reference case with five struts the strut losses approximately equal the duct losses.

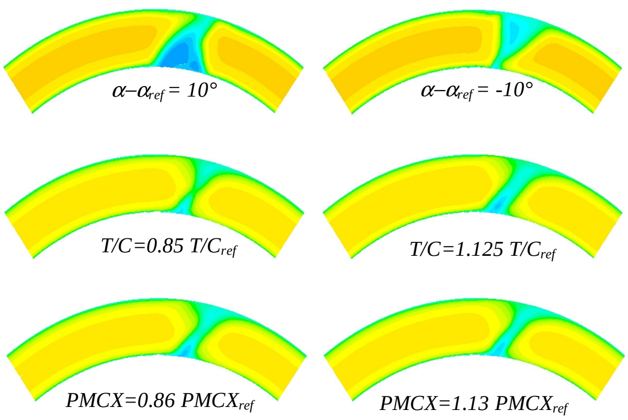

Fig.4. Total Pressure contours at the strut exit plane for different α (top), *T/C* ratios (middle) and PMCX values (bottom).

The generated database can be extended with experimental data from literature [9, 11]. The uncertainty in the prediction of the aerodynamic ITD performance is ultimately related to the large number of influencing parameters. After the selection of the duct parameters during the preliminary design iterations, a subsequent shape optimisation is necessary as illustrated in figure 5.

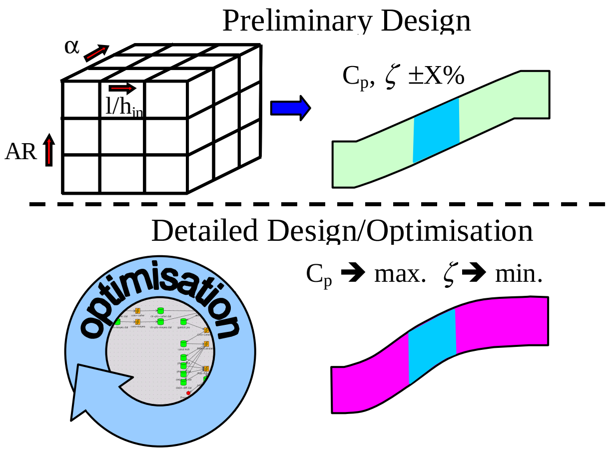

Fig.5. Sketch of the ITD design process.

3 Methodology

The first step in the shape optimisation process is the parameterisation. A multilevel parameterisation with familiar engineering parameters for the preliminary design and purely mathematical parameters for the subsequent detailed design has been chosen. The selection of the optimisation parameters has to be done with care to reduce the computational burden of 3D CFD calculations for the optimisation.

3.1 Test Case

The test case is a clean s-shaped duct with an area ratio of AR=1.35 and a non-dimensional length of L/h_i =4. A look at the Sovran and Klomp chart in figure 2 reveals that the duct (indicated by a blue dot) is conservative. The inlet conditions chosen are engine representative in terms of inlet Mach number, swirl angle and the 1D radial profiles of total pressure and temperature.

3.2 Duct Parameterisation

The duct geometry can be described by two types of parameter sets: the characteristic parameters are the area ratio AR, the duct length L, the inlet hub radius r_{1h} and the mean radius ratio r_2/r_1. These parameters, which are generally used in the preliminary design, determine roughly the pressure recovery and the pressure loss of the clean, vaneless duct [8]. The second parameter set defines the contour of the hub and the casing between the duct inlet and exit plane. The shape of the duct becomes important for the design of compact, aggressive intermediate ducts, which operate close to separation. The variation of the local curvature may hereby suppress the risk of boundary layer separation at the casing. In contrast to the characteristic parameters, the parameters of the second parameter set are by nature less intuitive and are for this reason more suitable for a design optimisation than for a classical design by analysis approach.

Two parametric representations commonly used in aerodynamic shape optimisation have been investigated. Both methods employ open cubic B-splines:

$$\mathbf{x}(t) = \sum_{\mathbf{i=1}}^{p} \mathbf{B}_i N_i^4(t) \qquad t \in [0,1] \qquad (4)$$

to generate the duct geometry. Their local control property and C^2-continuity make them attractive for geometry modification. The number of independent p parameters, which is equal for both methods, has been deliberately chosen to cover a large design space with a minimum number of parameters.

3.2.1 Camber line and Thickness

The duct geometry can be described by the definition of the duct mean line for which the height or area distribution is superimposed to define the duct end walls. This approach, which is derived from aerofoil design, is known as the camber line and thickness method [12, 13]. The mean line and height distribution of the baseline duct has been approximated by B-spline curves with five-control points. Only the inner control-vertices in figure 6 are allowed to move in a predefined range to avoid unrealistic duct shapes and to keep the main characteristic duct parameters unchanged. As a result, a total of eight parameters have been retained for the design of experiment (DOE).

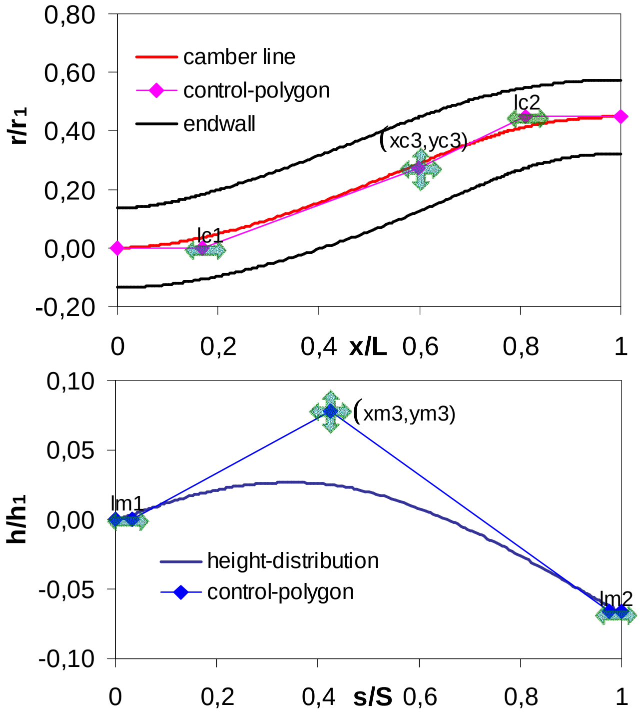

Fig.6. Duct Meanline and Height Distribution

It has to be noted that this approach may not preserve the C^1-continuity of the annulus at the duct inlet and exit plane. However, the generated duct end walls are smooth curves.

3.2.2 Hub and Casing Parameterisation

An alternative approach to describe the duct geometry is the definition of the hub and casing end wall independently. This approach is similar to the decoupling of the pressure and suction surface definition used in the design optimisation of highly loaded aerofoils [1, 14]. Each curve is again described by a B-spline curve with five-control points. The tangency condition at the B-spline endpoints limits the degree of freedom to four for each curve. The displacement direction for the inner control vertices of the casing and hub end wall is shown figure 7. The decoupling of the hub and casing end wall may result in a non-monotonic stream-wise area distribution. The total number of independent variables of p=8 of both methods is far too high for a practical design optimisation using a computational expensive 3D Navier-Stokes solver.

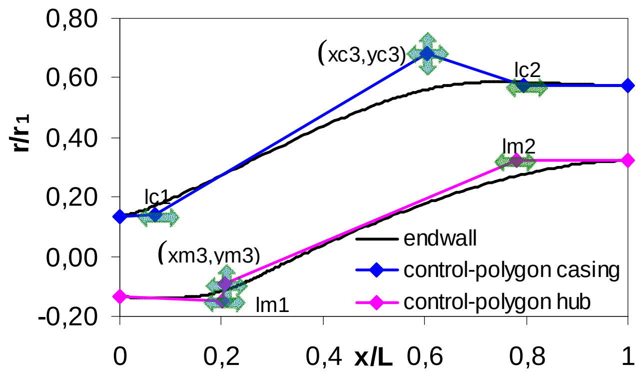

Fig.7. Hub and Casing Distribution

A DOE study has therefore been conducted:

- to determine the sensitivity of each parameter on the pressure recovery and total pressure loss and to identify significant parameter interaction,
- to determine the dependence between both pressure recovery and pressure loss and
- to define the optimisation strategy for each method.

3.3 Design of Experiments

A DOE study intends to extract as much information as possible about the correlation between the input variables and the one or multiple objectives from few computational experiments. Several sampling techniques exist that distribute the parameters across the design space. A comprehensive review of the different DOE techniques is given in [15]. Two techniques have been investigated. The central-composite design (CCD) locates the sample points on the edges of the design space to minimise the effects of random error and in the centre of the design space to capture non-linear system response. One drawback of this technique is the rapid increase of the number of samples m with the dimension p of the design space according to $O(2^P)$. This means that for p=8 more than 256 CFD runs have to be performed for the DOE study. A lower number of experiments is generally required for the Latin Hypercube sampling (LHS), which places the samples on the interior of the design space.

Each parameter range is hereby divided in *m* non-overlapping intervals on the basis of equal probability. The *m* randomly selected values of the first parameter are then paired with the *m* randomly selected values of the second parameter and so on until an *m* *p*-tuplet is formed. The final Latin hypercube sample contains one point in each of the intervals for each of the parameters. An example for the design exploration space for both techniques is shown in figure 8.

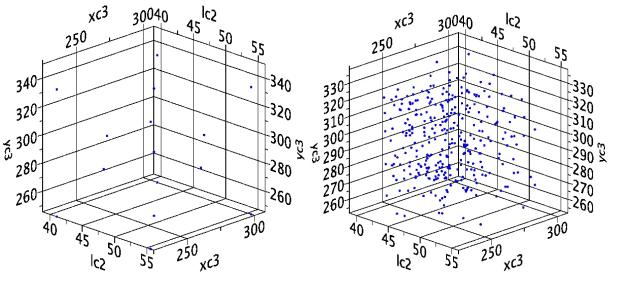

Fig.8. Sample Distribution of CCD (left) and LHS (right)

It becomes evident that the CCD sampling generates geometrically more extreme design than LHS.

3.3.1 Computational Model

A batch procedure enables the creation of the duct geometric model, the mesh generation, the CFD calculation and the data analysis in an automatic way. The setup of the workflow and the execution of the DOE study are realised using the commercial software tool LMS OPTIMUS V5.1. The CFD predictions have been carried out using Fluent V6.2. Axis-symmetric flow with swirl is considered for the duct flow. An Euler-implicit scheme for the time discretisation of the coupled equations has been chosen combined with a second-order upwind scheme for the convective fluxes. Menters popular SST model, which is recommended by the QNET-CFD best practice advice [16] and successfully applied for diffuser flow prediction [17, 18], has been employed for turbulence closure. Radial profiles for total pressure, total temperature and swirl angle have been imposed at the duct inlet. At the exit plane the target mass flow together with the radial equilibrium pressure distribution has been specified. The convergence criteria adopted are a four orders of magnitude reduction in average residual of density and an inlet-exit mass flow difference lower than 0.3%. The automatically generated structured grid shown in figure 9 has 160x130 cells and is refined close to the end walls to ensure an $y^+ \approx 1$ for near wall grid cells.

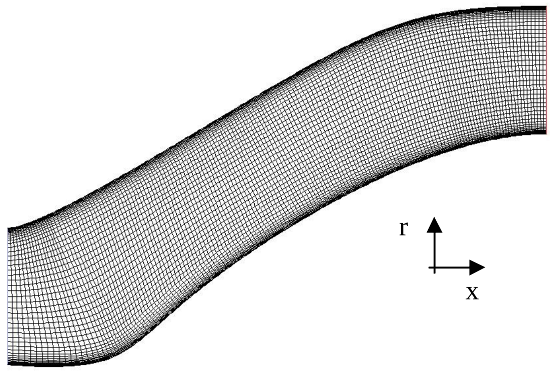

Fig.9. Computational Grid for a DOE sample

3.3.2 DOE Results

The DOE study with either CCD or LHS sampling has been carried out for the camber line and thickness parameterisation as well as for the hub and casing parameterisation. A second order response surface approximation (RSA) is constructed for each of the four DOEs. The required number *m* of CFD runs to train the RSA polynomials is given by [19]:

$$m > q = \binom{p+2}{2} \qquad (5)$$

The corresponding coefficients are determined from a least-square minimisation. The good-ness of fit criterion for the approximation is the adjusted coefficient of determination R_a^2. For the pressure loss for example this regression diagnostic value is defined by:

$$R_a^2 = 1 - \frac{\sum_{i=1}^{m} (\zeta_i - \hat{\zeta}_i)^2}{S(\zeta)(m-q)}, \qquad (6)$$

where ζ_i is the calculated loss, $\hat{\zeta}_i$ represents it's approximated value and $S(\zeta)$ is the standard deviation of ζ. Each of the DOEs has a R_a^2 value of higher than 0.985 for both objective functions C_p and ζ, which indicates a high quality RSA.

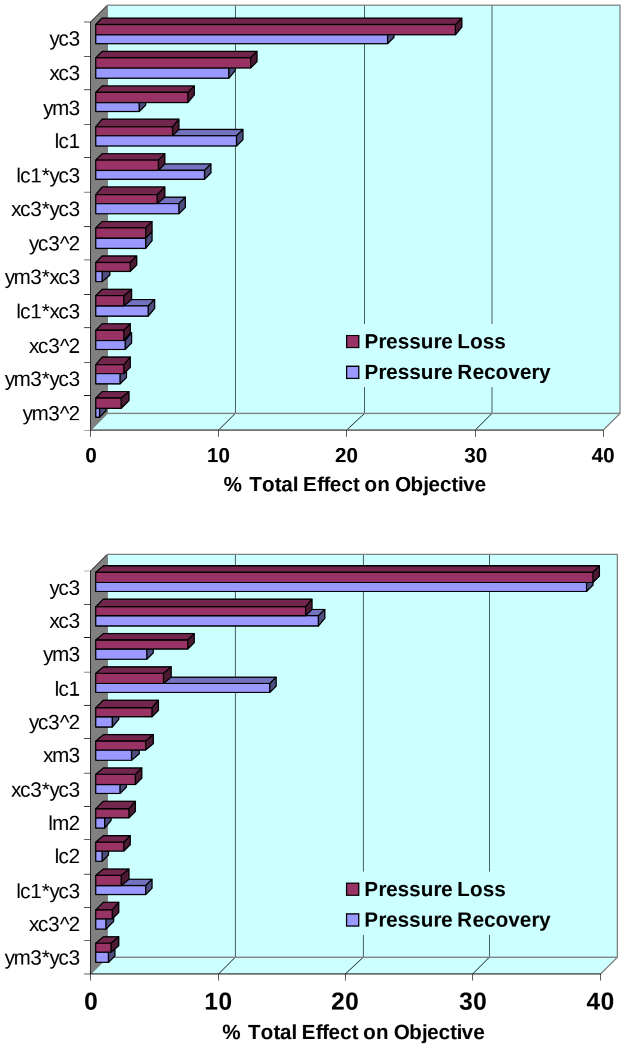

Fig.10. Pareto chart for camber line/thickness (top) and casing/hub (bottom) parameterisation

The Pareto chart in figure 10 graphically summarizes and displays the relative importance of each RSA coefficient on the objective functions. The results are obtained with the LHS sampling. Only the twelve most dominant coefficients are shown. The camber line and thickness parameterisation has many non-linear coefficients with a significant effect on the response. Furthermore, the strong presence of off-diagonal elements among the top 12 coefficients shows a cross-correlation between the design parameters. By contrast, the RSA of the hub and casing parameterisation is dominated by relatively few coefficients for the linear polynomials. The biggest contributors on the objective are the co-ordinates of the inner control vertex of the casing *(xc3, yc3)*, which define the casing curvature and hence the acceleration of the casing boundary layer after the first bend. The influence of cross-correlation coefficients on the RSA is negligible. The influence of the sampling method on the generated RSA can be seen in figure 11. There are only minor differences in the parameter ranking. The RSA is hence independent of the sampling technique. This clearly favours LHS over CCD, because of it's better robustness and lower sample number.

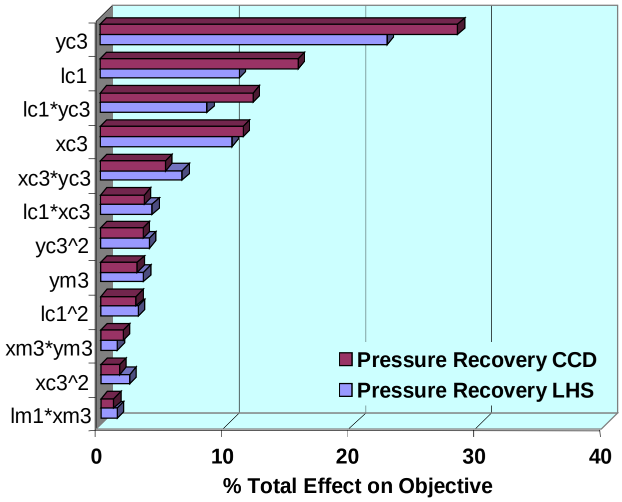

Fig.11. Pareto chart for CCD and LHS for the camberline and thickness parameterisation

Both parameterisation methods show a rather tight correlation for the pressure recovery and pressure loss depicted in figure 12 for LHS and the casing and hub parameterisation. This makes the design of a strutless ITD with a high pressure recovery and a low pressure loss challenging.

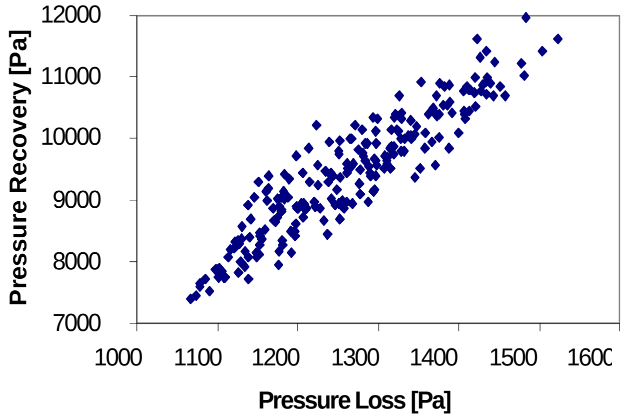

Fig.12. Correlation between C_p and ζ

An important result for the ITD design is also the fact, that the C_p and ζ variations in figure 12 are in the range of ±/35% and ±/50% respectively of the mean value for the investigated test case. This demonstrates the limitations of the preliminary design assessment for which only the characteristic parameters are defined. It also shows the potential gain by an optimisation of the duct end walls.

The camber line and thickness parameterisation only allows on a limited scale a parameter reduction due to their more equal contribution to the value of the objective function. The interaction between the design parameter is a result of the coupling of the end walls. A local control of either the hub or casing contour is not feasible. Another more serious disadvantage of the method for the application in a design system is the potential violation of the C^1-continuity of the annulus at the duct inlet and exit plane. The parameterisation of the duct end walls respects this constraint. The linear dependence of the objective function on the design parameters and their lack of interaction suggests the use of a gradient based research method for the duct optimization in lieu of a surrogate model like the RSA, which is computational expensive to generate.

4 Design application

The reduced parameter set for the hub and casing end wall has been employed for the ITD shape optimisation in order to demonstrate the potential benefit of the method in the duct design process.

4.1 Test case

The test case displayed in figure 13 is a high diffusion strutless ITD with a duct area ratio of 1.31 and the non-dimensional length l/h_1= 1.81. The aggressive duct (red dot in figure 2) is currently tested at the transonic test turbine facility [3] of Graz University of Technology. The measured radial profiles of total pressure, total temperature and swirl angle are imposed at the duct inlet.

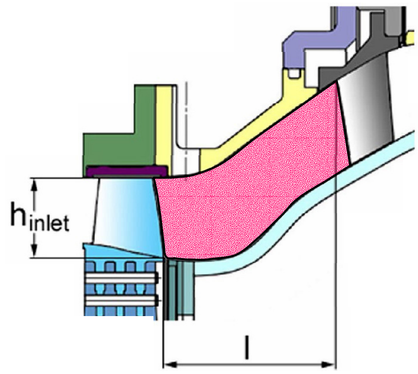

Fig.13. Aggressive ITD of TU Graz from [3]

The control polygons of the baseline duct for the test case have been generated by simply placing the control-point vertices of the casing and hub end wall in each case on a cubic curve $r=r(x)$, which is defined by the casing or hub endpoints and the associated slopes. The C^2-continuity at the duct interfaces is hence ensured.

A DOE study with LHS sampling has been conducted for the duct with similar results for C_p and ζ and the parameter ranking as shown in figure 10. The results of the DOE study are obviously independent of the characteristic duct parameters. This confirms that the selected parameters are suitable for the duct optimisation.

4.2 Duct Optimisation

The design task is to optimise the pressure recovery of the ITD duct without an increase of the pressure loss. The corresponding formulation of the objective function is hence:

$$Obj = \omega_1 \frac{Cp - Cp_{ref}}{Cp_{ref}} + \omega_2 \frac{\zeta_{ref} - \zeta}{\zeta_{ref}} \rightarrow \text{max.} \qquad (7)$$

No constraint has been applied for the objective function. The parameters used for the optimisation are the four most important parameters shown in figure 10, which are the inner control vertex of the casing *(xc3,yc3)*, the tangential length *lc1* and the hub co-ordinate point *ym3*. The optimisation method is the gradient-based sequential quadratic programming algorithm. The CFD solver and process integration platform employed are the same than for the DOE study.

4.3 Results

The optimised duct contour is shown in figure 14. The result is obtained after approximately 50 CFD runs. The optimisation progress has a non-linear, degressive growth, which refers to a flat optimum.

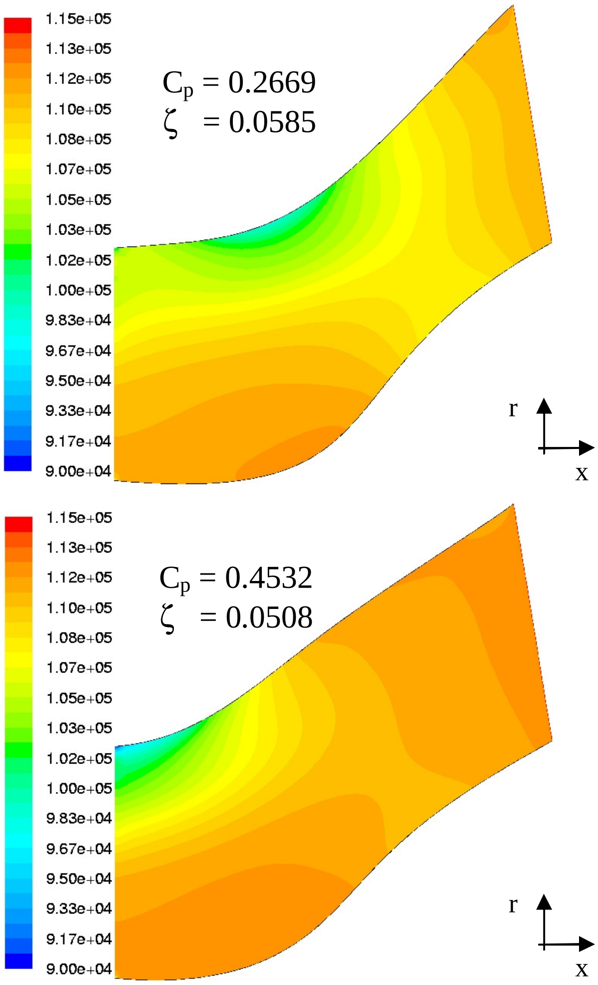

Fig.14. Static pressure contour plot of baseline (top) and optimised duct (bottom)

Compared to the baseline duct, the inflection point of the hub end wall is moved forward as well as the minimum radius of curvature of the casing end wall. Therefore the casing flow acceleration is confined to the inlet plane. This increases the static pressure difference between hub and casing at the duct inlet. The mass averaged inlet Mach number however increases only slightly by +0.02. The area distribution of the duct along the camber line depicted in figure 15 shows, that the optimised duct still has a non-monotonic area change but the duct throat has considerably increased.

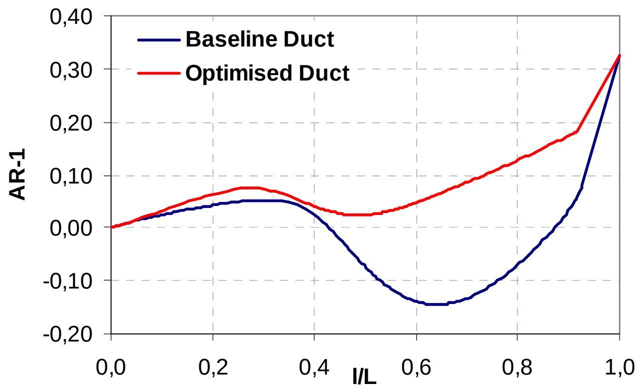

Fig.15. Area distribution of baseline and optimised duct

The exit Mach number distribution in figure 16 indicates that the flow migrates from the outer to the inner wall. The radial flow distortion is yet preserved.

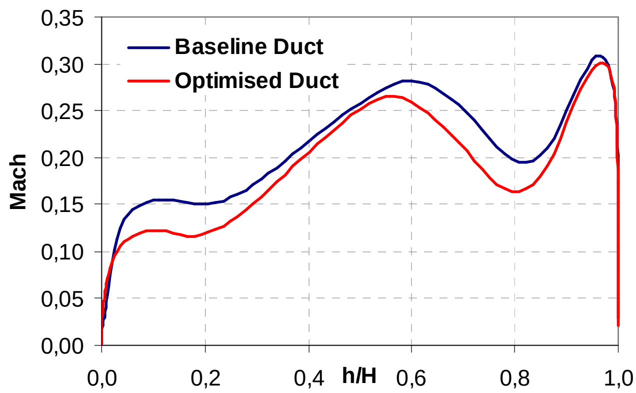

Fig.16. Mach number profile at duct exit plane

The total pressure loss finally has been reduced from ζ=0.0585 to ζ=0.0508, whereas the pressure recovery increases from C_p=0.267 to C_p=0.4532. This result is apparently inconsistent with the linear C_p-ζ correlation found before. However, it is still in the scatter of figure 12.

5 Conclusions

The parametric design and optimisation of S-shaped ducts has been presented. A two-level duct parameterisation has been chosen to meet the requirements for preliminary and detailed design. A systematic CFD study has been conducted to establish a database for the preliminary design of ducts with swirling flow and struts. The study has shown the importance of the strut generated losses on the duct performance. Two alternative parametric representations of the duct end walls have been investigated. The results of the DOE study show that due to the decoupling of the casing and hub end wall the number of design parameters can be halvened with a close coupling between design parameters and objective function. The duct is very sensitive to changes of the casing end wall. The optimisation of the clean duct resulted in a significant increase of pressure recovery without degradation of the pressure loss. However, a 3D CFD calculation has to be performed in order to verify the optimisation results. The computational domain should hereby also include the upstream HPT to assess the effect of the radial pressure gradient change caused by the optimised duct. The impact of the strut on the duct flow needs applications to be considered in future research for a practical application of the design optimisation.

Acknowledgements

The current work was supported by the EU project AIDA (**A**ggressive **I**ntermediate **D**uct **A**erodynamics, Contract: AST3-CT-2003-502836) and Turbomeca (SAFRAN Group). Their permission to publish this paper is gratefully acknowledged. The authors would also like to thank H.Vignau and R.Thomas for their assistance in the paper preparation.

References

[1] Küsters B., Schreiber H.A., Köller U. and Mönig R.. Development of Advanced Compressor Airfoils for Heavy-Duty Gas Turbines— Part I: Design and Optimization. *ASME Journal of Turbomachinery*, Vol. 122, Iss.3, pp. 406-414, 2002.

[2] Haselbach F., Schiffer H.P., Horsman M., and Dressen S., Harvey N. and Read S.. The Application of Ultra High Lift Blading in the BR715 LP Turbine. *Proceedings of ASME Turbo Expo 2003*, Atlanta, USA, GT2003-38174, pp 1-13, 2003.

[3] Göttlich E., Malzacher F., Heitmeir F. and Marn A.. Adaptation of a Transonic Test Turbine Facility for Experimental Investigation of Aggressive Intermediate Turbine Duct Flows, *Proceedings of ISABE 2005*, Munich, Germany, ISABE-2005-1132, pp 1-8, 2005.

[4] Norris G., Dominy R.G. and Smith A.D.. Strut Influences Within a Diffusing Annular S-Shaped Duct. *Proceedings of ASME Turbo Expo 1998*, Stockholm, Sweden, 98-GT-425, pp 1-9, 1998.

[5] Miller R.J., Moss R.W., Ainsworth R.W. and Harvey N.W.. The development of turbine exit flow in a swan-necked inter-stage diffuser/. *Proceedings of ASME Turbo Expo 2003*, Atlanta, USA, GT2003-38174, pp 1-13, 2003.

[6] Sovran G., and Klomp, E.D.. Experimentally Determined Optimum Geometries for Rectilinear Diffusers with Rectangular, Conical or Annular Cross-Section. *Fluid Mechanics of Internal Flow*, 1st edition, Elsevier, pp 270-319, 1967.

[7] Becker B.. Untersuchung der Strömung in beschaufelten Brennkammerdiffusoren unter dem Einfluss angrenzender Gasturbinenkomponenten, Dissertation, Technische Universität Darmstadt, Darmstadt, pp 1-121, 2005.

[8] Japikse, D.. Correlation of Annular Diffuser Performance with Geometry, Swirl, and Blockage. *Proceedings of the 11th NASA/OSU Thermal and Fluids Analysis Workshop*, Cleveland, USA, NASA/CP-2002-211-486, pp 107-118, 2002.

[9] Feldcamp, G.K. and Birk A.M.. Strut losses in a diverging diffuser with swirling flow, *Proceedings of ASME Turbo Expo 2006*, Barcelona, Spain, GT2006-90566, pp 1-10, 2006.

[10] Vassiliev V., Irmisch S., Richardson D.P. and Claridge M.. Experimental and Numerical Investigation of the impact of swirl on the performance of industrial gas turbine exhaust diffusers, *Proceedings of ASME Turbo Expo 2003*, Atlanta, USA, GT2003-38424, pp 1-11, 2003.

[11] Lohmann, R.P., Markowski S.J., and Brookman, E.T.. Swirling Flow Through Annular Diffusers with Conical Walls, Journal of Fluids Engineering, Vol. 101, pp. 224-229, 1979.

[12] Miller P.L., Oliver J.H., Miller D.P. and Tweedt D.L.. BladeCAD: An Interactive Geometric Design Tool for Turbomachinery Blades, NASA Technical Memorandum 107262, pp 1-8, 1996.

[13] Casey, M.V.. A computational geometry for the blades and internal flow channels of centrifugal compressors. *ASME Journal of Engineering for Power*, Vol.105, pp 288-295, 1983.

[14] Gräsel J., Keskin A., Swoboda M., Przewozny H., Saxer A.. A full Parametric Model for Turbomachinery Blade Design and Optimisation. *Proceedings of ASME DETC 2004 30th Design Automation*

Conference, Salt Lake City, USA, DETC2004-57467, pp 1-8, 2004.

[15] Giunta A., Wojtkiewicz S. F. and Eldred M.. Overview of Modern Design of Experiment Methods for Computational Simulations, Proceedings of the 41st AIAA Aerospace Science Meeting and Exhibit, Reno, USA, AIAA-2003-0649, pp 1-17, 2003.

[16] Casey, M.V.. Best Practice Advise for Turbomachinery Internal Flows, QNET-CFD Network Newsletter, Vol. 2, No. 4, pp 1-7, 2004.

[17] Hellsten A. and Laine S.. Explicit Algebraic Reynolds-Stress Modeling in decelerating and separating flows. AIAA-2000-2313, pp 1-13, 2000.

[18] Xiao Q., Tsai H.M. anf Liu F.. Computation of Transonic Diffuser Flows by a lagged k-ω Turbulence Model. *AIAA Journal of Propulsion and Power*, Vol.19, pp 473-483, 2003.

[19] Madsen J. I., Shyy W. and Haftka R.T.. Response Surface Techniques for Diffuser Shape Optimization. *AIAA Journal*, Vol. 38, No. 9, pp 1512-1518, 2000.